AJNR

Experimental Autoimmune Encephalomyelitis in the Rat Spinal Cord: Lesion Detection with High-Resolution MR Microscopy at 17.6 T

Andreas Steinbrecher, Thomas Weber, Thomas Neuberger, André M. Mueller, Xiomara Pedré, Gerhard Giegerich, Ulrich Bogdahn, Peter Jakob, Axel Haase and Cornelius Faber

AJNR Am J Neuroradiol 2005, 26 (1) 19-25
http://www.ajnr.org/content/26/1/19

Experimental Autoimmune Encephalomyelitis in the Rat Spinal Cord: Lesion Detection with High-Resolution MR Microscopy at 17.6 T

Andreas Steinbrecher, Thomas Weber, Thomas Neuberger, André M. Mueller, Xiomara Pedré, Gerhard Giegerich, Ulrich Bogdahn, Peter Jakob, Axel Haase, and Cornelius Faber

BACKGROUND AND PURPOSE: **Experimental autoimmune encephalomyelitis (EAE) is an inflammatory demyelinating disorder of the CNS and an animal model of multiple sclerosis. We used high-field MR microscopy at 17.6 T to image spinal cord inflammatory lesions in the acute stage of chronic relapsing rat EAE. We sought to compare lesions detected on MR imaging with histopathologic findings and to quantify the inflammatory lesion load.**

METHODS: **Imaging of fixed spinal cord specimens was performed by using a 3D gradient-echo sequence with a spatial resolution of 35 × 35 × 58 μm^3 and a total imaging time of 5.5 hours. Histopathologic analysis was performed by staining axial sections with hematoxylin-eosin or Luxol fast blue to identify cellular infiltration and demyelination.**

RESULTS: **Clinical signs of EAE occurred on days 10–14 after immunization. On day 22, healthy white matter and gray matter were differentiated by high contrast on T2*-weighted images, with white matter lesions appearing as hyperintense areas in the normal-appearing white matter. Inflammatory lesions identified on histopathologic evaluation were readily detected with MR imaging and vice versa. MR imaging and histopathologic analysis had excellent correlation regarding the extent of white matter lesions. Inflammatory infiltrates of gray matter were not detectable with MR imaging. Using a semiautomatic segmentation of the acquired MR data, we could quantify white matter lesion load.**

CONCLUSION: Ex vivo **high-resolution MR microscopy of the spinal cord at 17.6 T allows rapid and highly accurate determination of CNS inflammation by demonstrating virtually all histologically detectable white matter inflammatory lesions.**

MR imaging is a powerful, noninvasive means to detect brain and spinal cord lesions in inflammatory disorders of the CNS. It has become the most important paraclinical technique in the diagnosis and subsequent monitoring of multiple sclerosis (MS) (1, 2). However, because of the extremely limited availability of data on lesions defined with both MR imaging and histopathologic analysis, MR imaging is not yet helpful in differentiating the recently identified pathologic and potentially pathogenetic subtypes of MS (3–5).

The variants of experimental autoimmune encephalomyelitis (EAE), the prime animal model of MS, each reflect given subtypes better than others and thus offer themselves for the investigation of specific questions with respect to immune pathogenesis, lesion evolution, and therapeutic developments (6–8). Therefore, MR microscopy performed in EAE models offers a unique opportunity for research to integrate pathologic and MR imaging lesion morphology on a given immunopathogenetic background.

All *in vivo* MR studies in rodent EAE have involved the imaging of brain lesions (9–17), thereby circumventing the technical difficulties of experimental spinal cord imaging. Furthermore, only two systematic, *ex vivo* MR studies of fixed postmortem spinal cord samples have been reported, to our knowledge. These studies were performed with a

Received February 10, 2004; accepted after revision April 26.

From the Department of Neurology, University of Regensburg (A.S., A.M.M., X.P., G.G., U.B.), and the Germany and Physikalisches Institut, EP5, University of Wuerzburg (T.W., T.N., P.J., A.H., C.F.), Germany.

A.S. and T.W. made equal contributions to this work.

Supported in part by grants from the Deutsche Forschungsgemeinschaft GI 323–1/1–2 (to G.G.) and DFG Ha 1232/13 (to A.H.).

Presented in part at the Annual Meeting of the ESMRMB, Cannes, 2002; the 5th Annual Meeting of the German section of ISMRM, Hamburg, 2002; the meeting of ISMRM, Toronto, 2003; and the 7th International Conference on Magnetic Resonance Microscopy, Snowbird, UT, 2003.

Address correspondence to: Andreas Steinbrecher, MD, Department of Neurology, University of Regensburg, Universitaetsstr 84, D-93053 Regensburg, Germany.

weak magnetic field or in the mouse (18, 19); both of these approaches limit the morphologic information. In past years, the spatial resolution of MR imaging has improved considerably as higher field strengths have become available. This advance has resulted in a higher net equilibrium magnetization and therefore an improved signal-to-noise ratio (SNR).

Using a model of chronic relapsing EAE, we hypothesized that *ex vivo* high-field MR microscopy enables visualization of virtually all inflammatory lesions that can be detected histopathologically and that it provides a rapid and accurate means to determine the lesion load.

Methods

EAE Induction

All procedures were conducted according to protocols approved by the animal care committee of our medical faculty. We obtained 10 female Dark Agouti rats (Harlan Winkelmann, Borchen, Germany), which were 10 weeks of age when used for the experiments. The *N*-terminal fragment of rat myelin oligodendrocyte glycoprotein (MOG) containing the amino acids 1–125 (cDNA obtained as a gift from C. Linington, Martinsried, Germany) was expressed in *Escherichia coli* and purified to homogeneity by means of nickel chelating chromatography, as described elsewhere (20). The purified protein was dialyzed against phosphate-buffered saline (PBS). To induce active EAE, eight rats were intradermally immunized at the base of the tail with an inoculation volume of 200 μL containing 65 μg of recombinant MOG(AA1–125) in PBS and an equal volume of incomplete Freund adjuvant supplemented with 400 μg of H37RA. Rats were examined and graded daily on a scale of increasing disease severity as follows: 0 was no signs; 0.5, partial tail weakness; 1, a limp tail; 2, partial hindlimb weakness or hemiparesis; 3, complete paralysis of at least one hindlimb; 4, forelimb weakness; and 5, moribund or dead. Two non-immunized rats were used as controls.

Sample Processing

Rats were sacrificed on day 22 after immunization with a transcardial perfusion with 0.9% saline followed by 4% paraformaldehyde. The intact vertebral column was placed into fixative and stored at 4°C. Before imaging, the spinal cords were excised and cut into cervical, thoracic, and lumbosacral segments. These samples were placed in 5-mm MR tubes containing 4% paraformaldehyde. The debubbled sample was fixed with a plug inside the tube to prevent motion artifacts.

MR Imaging

Imaging experiments were conducted at 17.6 T (750-MHz proton resonance frequency). The system (750WB Avance; Bruker Biospin, Rheinstetten, Germany) was equipped with a 1-T/m gradient system with an inner diameter of 40 mm and a rise time of 100 μs. A commercial linear 5-mm ^{1}H birdcage resonator was used for excitation and for the detection of signal intensity.

For high-resolution imaging, several combinations of TE, TR, and acquisition bandwidth were tested, both for spin-echo and gradient-echo sequences. The best SNR and contrast-to-noise ratio (CNR) was achieved by using a spoiled 3D gradient-echo sequence with a TR/TE of 50/13.5 and a 25 ° hard pulse for excitation (21). This combination of TR, TE, and flip angle resulted in moderate T1 weighting and strong T2* weighting. The field of view of $5 \times 5 \times 15$ mm^3 and acquisition matrix of $128 \times 128 \times 256$ yielded a spatial resolution of $35 \times 35 \times 58$ μm^3. With 24 signal intensity averages, sections were obtained in 5.5 hours. Data were collected of the cervical, thoracic, and lumbar portion of the spinal cords.

Histopathologic Analysis

A series of histologic sections from selected rats used for the imaging experiments was prepared for pathologic evaluation and comparison with the MR microscopic images. After imaging, paraffin-embedded sections of 6-μm thickness were cut in the axial plane throughout the cervical, thoracic, and lumbar segments of the spinal cord. Adjacent sections were stained with hematoxylin-eosin (HE) and Luxol fast blue (LFB) to identify cellular infiltration and demyelination, respectively. Histopathologic sections were matched with MR images by using the perforation landmark on MR images, the shape and size of the spinal cord, the configuration of the gray matter according to the atlas of Paxinos and Watson (22), and the presence and configuration of the lesions.

3D Visualization

3D image reconstruction and visualization was performed (Amira 2.3; TGS, San Diego, CA). Segmentation was done semiautomatically by using the lasso tool (Amira; TGS), which enabled the detection of borderlines. User interaction was necessary because of CNR variations across the sample due to B1 field inhomogeneities in the radiofrequency resonator.

Results

Clinical Status

All immunized rats developed signs of EAE by day 14 (range, days 10–14). At the time of perfusion on day 22, all rats had developed EAE, with the most severely affected rat showing grade 4 disease (i.e., complete hindlimb and partial forelimb paresis).

Imaging Results

Imaging was performed with specimens from seven rats with differing EAE-severity (grade 2 or more) and from two nonimmunized control rats. There was a generally good correlation between clinical score and lesion load, as determined with MR imaging (data not shown), although this was not formally studied. Imaging results from both MR imaging and histopathologic analysis are presented from one EAE rat with grade 4 disease and a healthy control rat.

Figures 1A and 2A show anatomic MR images from the thoracic and lumbar spinal cord of the healthy control rat in longitudinal and axial orientation, respectively. On T2*-weighted MR images, spinal cord gray matter and white matter were easily differentiated with SNRs of 31 and 13, respectively, yielding a CNR of 18. Normal white matter and gray matter appeared dark gray and light gray, respectively.

Spinal cord lesions in the rat with grade 4 EAE were visible on both T2*-weighted gradient-echo and T2-weighted spin-echo images. Figures 1 and 2 also show longitudinal and axial MR images from lumbar, thoracic, and cervical spinal cord levels in a rat with EAE grade 4. On T2*-weighted images, lesions in the white matter were seen as hyperintense areas indicating an increase in tissue water content consistent with

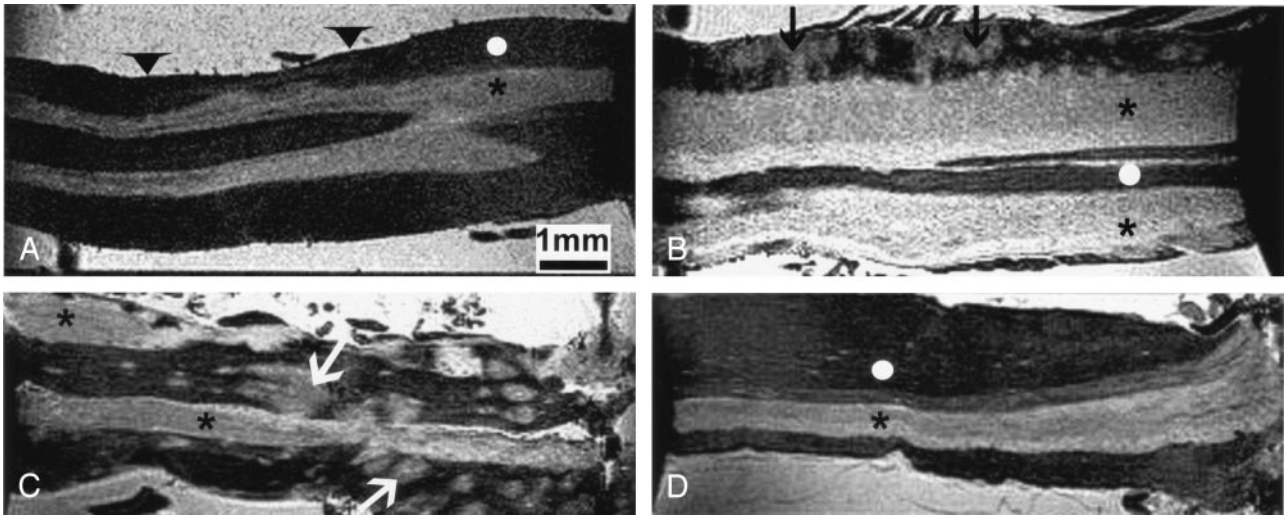

FIG 1. Sagittal MR images of rat spinal cord. *Arrowheads* indicate the cord surface; *asterisks*, gray matter; *white circle*, white matter; and *arrows*, lesions.

A, Thoracic cord in a control rat.

B–D, Lumbar (*B*), thoracic (*C*), and cervical (*D*) sections in a rat with grade 4 EAE.

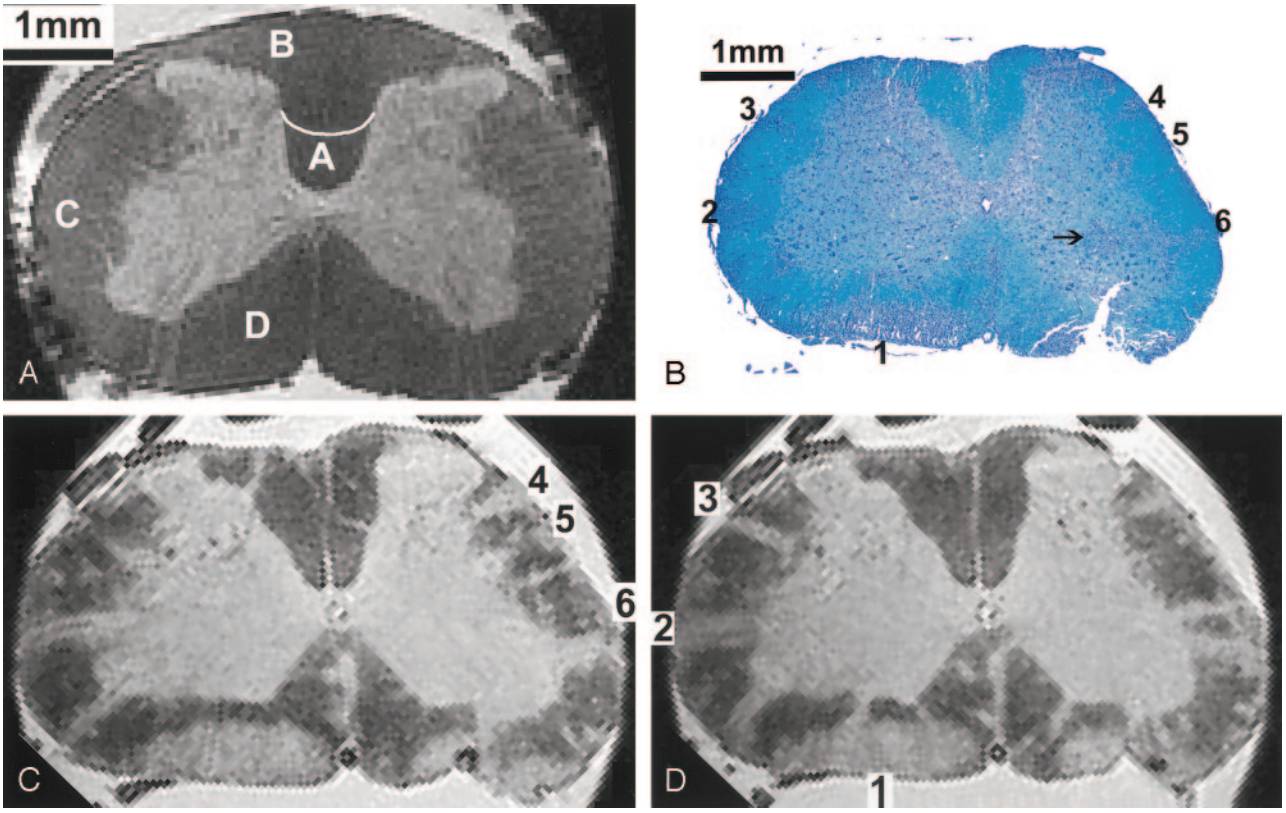

FIG 2. Axial MR and histopathologic images of rat spinal cord.

A, Lumbar cord in a control rat. Letter *A* indicates the corticospinal tract; *B*, gracile fasciculus; *C*, lateral funiculus; and *D*, anterior/ventral funiculus.

B–D, Lumbar portion (L3) in a rat with grade 4 EAE. Multiple lesions (*1–6*) can be identified in the anterior and lateral parts of the white matter. Histologic section (LFB stain) in *B* shows an inflammatory infiltrate in the gray matter (*arrow*). Corresponding MR images in C and *D*, spaced 150 μm, account for the slightly different orientation of the axial plane introduced by histologic processing. Lesions *1–6* in *A* are shown.

the presence of cellular infiltrates, demyelination, or edema. MR images were scaled to show the best contrast between lesions and normal-appearing white matter. The CNR between normal-appearing white matter and white matter lesions was 10. Lesions were generally located in the superficial and deep white matter, with the highest number observed in the lumbar part and fewer lesions in the thoracic segment. Lesions were absent in all but the most caudal part of the cervical cord sample (Fig 1B–D). For comparison, a

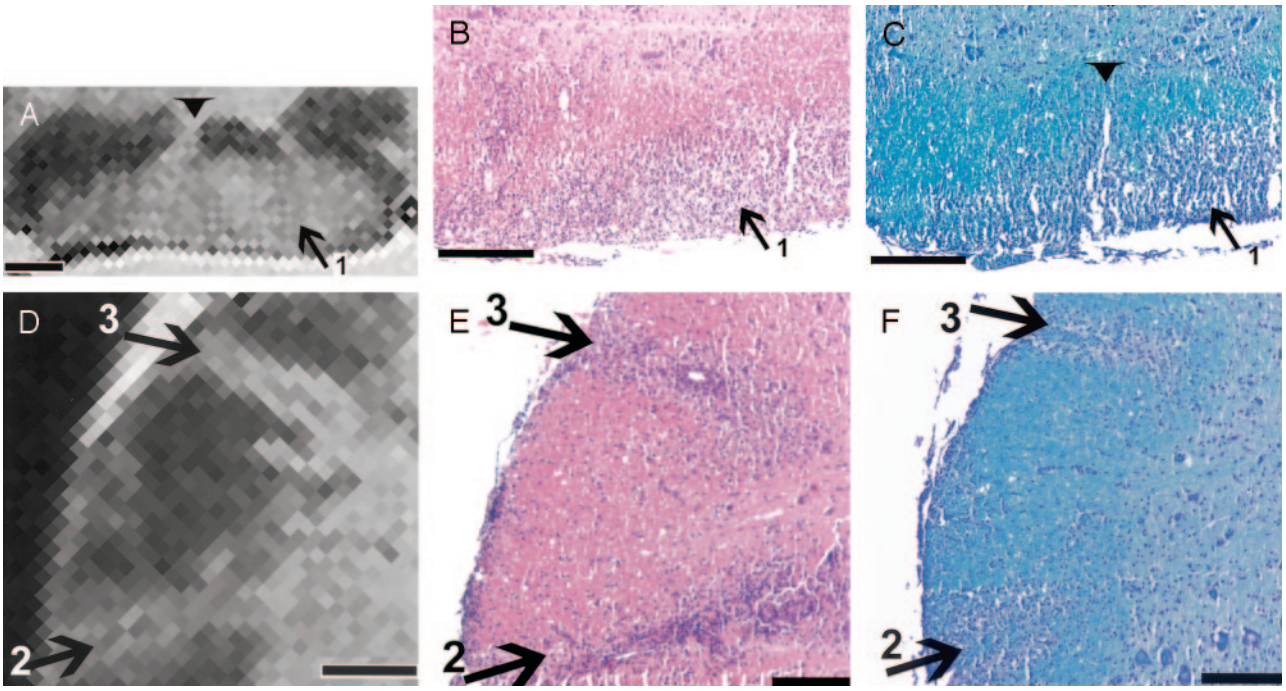

FIG 3. Lesion correlation in the ventral and lateral columns. *Bar* in *A–D*= 250 μm.
A and *D*, Details of the MR image in Figure 2D show a large lesion (*1*) in the ventral part of the cord (*A*) and two lesions (*2* and *3*) in the lateral part (*D*).
B, *C*, *E*, and *F*, Corresponding histologic sections stained for HE (*B* and *E*) and LFB (*C* and *F*) show the lesions depicted in A and Figure 2B. Note the fingerlike protrusion of lesion *1* (*arrowhead*) in *A* and *C*.

longitudinal MR image from the thoracic cord of the healthy control rat is shown; on this, no lesions were visible. Most of the lesions were found in the ventral (anterior) and lateral columns, as compared with the dorsal columns.

While lesions in mildly affected areas tended to be limited to the submeningeal or superficial white matter, lesions in more heavily involved areas extended to the boundary between white matter and gray matter, which was less well defined in diseased animals (Fig 2C and D). In the gray matter itself, no lesions were identified on MR imaging.

Histopathologic Analysis

Histopathologic analysis was carried out in the spinal cord specimens that were used for MR imaging to make a 1:1 correlation of the lesions. Lesions consisted of both cellular infiltration and associated demyelination. Infiltrates contained mostly macrophages and lymphocytes, with a few neutrophils. With regard to number, location, and shape, the inflammatory and demyelinating lesions detected on histopathologic results closely corresponded to hyperintense lesions on MR imaging. Lesions depicted on MR images were likewise found on the histopathologic sections. Even perivascular layers of only few cells caused visible lesions on MR images. These findings are exemplified in Figure 2 by the comparison of MR images with a corresponding low-power photomicrograph showing axial sections of the lumbar spinal cord with numerous lesions. Three lesion areas visualized on the axial MR image in Figure 2D were further analyzed. Individual lesions in these areas are shown on a magnified view to allow for more detailed comparison with the corresponding HE- and LFB-stained histologic sections (Figs 3 and 4). While every effort was made to produce MR images and histologic sections in the same perpendicular orientation with respect to the longitudinal axis of the spinal cord, small deviations were unavoidable. In addition, the aspect of small lesions (as visualized on histologic reports) tended to differ, even between adjacent sections.

Figure 3A shows a large lesion (lesion *1* from Fig 2B and D) in the right ventral column, with a fingerlike extension to the gray matter–white matter boundary. On the histologic sections (Fig 3B and C), both the cellular infiltration and the accompanying myelin loss were clearly seen. There was a rim of relatively unaffected tissue bordering the ventral horn, which could be identified by large neurons. The fingerlike protrusion seen on MR imaging corresponded to a perivascular infiltrate; this was best seen in Figure 3C, with the adjacent image (Fig 3B) being slightly out of plane.

Two hyperintense lesions extending from the surface to the gray matter–white matter boundary in the right ventrolateral and lateral area are shown in Fig 3D–F (lesions *2* and *3* from Fig 2B and D). Between these lesions and surrounding them, the white matter appeared uniformly dark and unaffected, with the exception of the submeningeal zone and a small su-

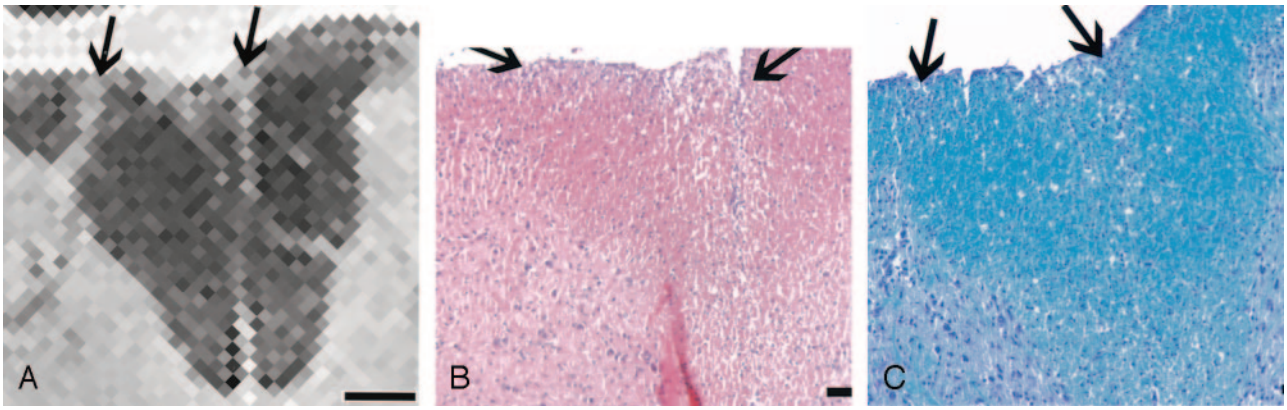

FIG 4. Lesion correlation in the dorsal column. *Bar* in *A* = 250 μm.
A, Detail of the MR image in Figure 2B shows only two small lesions (*arrows*).
B and *C*, Corresponding histologic sections stained for HE (*B*) and LFB (*C*) show. only a few inflammatory cells (*arrows*).

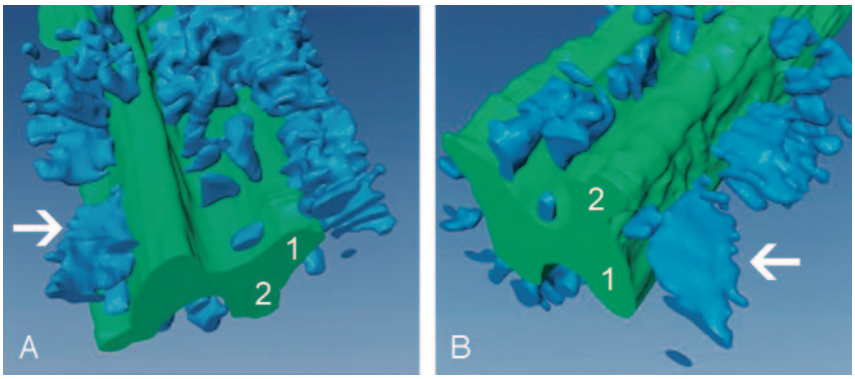

FIG 5. Lesion load quantification. 3D visualization of the thoracic spinal cord in the animal with grade 4 EAE. Gray matter is *green*; white matter lesions are *blue* (*arrow*); 1 is ventral horn; 2 is dorsal horn. Lesion load in the depicted cord is 16% of the white matter. Note the relative paucity of lesions in the dorsal part versus the ventral and lateral parts of the cord.
A, Ventrolateral view.
B, Dorsolateral view.

perficial and less-hyperintense zone between the two larger lesions. While the histologic sections confirmed the two large lesions, they also showed the submeningeal cellular infiltrate and a small infiltrate in the superficial white matter (Fig 3E and F).

The dorsal columns were the least-affected part of the spinal cord, as exemplified in Figure 4. On the histologic sections, loose clusters of inflammatory cells were seen close to the surface in the center and also on the right side of the dorsal columns. On the LFB stain in particular, a perivascular infiltrate composed of only a few cell layers was recognized; these extended deeply into the dorsal funiculus. The infiltrates were identified as moderately bright hyperintense lesions on MR imaging. Finally, the most central part of the dorsal columns (i.e., the area corresponding to the pyramidal tract) often appeared slightly hyperintense on MR images, but with a diffuse boundary in contrast to that of the aforementioned lesions. On the histologic sections, myelin staining was slightly paler, but there is no corresponding infiltration or demyelination (Fig 2B).

In severe EAE, lesions can extend into the gray matter as well. While this was also the case in the grade 4 rat presented here (Fig 2B), these gray matter lesions did not have sufficient contrast relative to healthy gray matter to be detectable in the MR images (Fig 2C and D).

3D Visualization and Lesion Load Quantification

3D reconstruction of the MR dataset from the thoracic spinal cord of the animal with grade 4 EAE was performed (Fig 5). On these images, gray matter was depicted in green and white matter lesions were light blue. Large lesion aggregates were easily seen throughout the white matter of the specimen. Furthermore, the 3D reconstruction illustrated the considerable longitudinal extension of the lesion, which is only partly seen on conventional longitudinal MR imaging sections (Fig 1B). In the region shown, the white matter lesion load, defined as the lesion volume divided by the total white matter volume, amounted to 16%. White matter volume versus gray matter volume in the scanned portion was around 2.9.

Discussion

We used high-field MR microscopy to image acute spinal cord inflammatory lesions in a model of chronic relapsing EAE in Dark Agouti rats and to compare lesions detected on MR imaging with those shown on histopathologic reports. High-resolution MR imaging data were obtained with a CNR of 10 between white matter lesions and healthy white matter. Lesions were best seen on conventional T2*-weighted images. More detailed lesion characteriza-

tion with differentiation between demyelination, inflammation, and axonal damage was not possible. Both inflammation and demyelination resulted in a T2* increase, and even more advanced MR techniques do not offer sufficient specificity. For example a decrease of the magnetization transfer ratio indicates myelin destruction or reduced axonal attenuation (4, 23). In an MR imaging study, Namer et al (24) compared demyelinating and nondemyelinating variants of EAE in Lewis rats and did not detect differences in unfixed samples, even by using magnetization transfer methods. Only sample dehydration allowed the detection of demyelination from T2 relaxation spectra and magnetization transfer data. In that study, however, only global spectra of spinal cord sections were examined; these gave no information about the distribution of demyelination.

We compared the feasibility and sensitivity of lesion detection by means of MR imaging with the criterion standard (i.e., histopathologic analysis). Direct visualization of EAE lesions on high-field MR microscopy was achieved in a total imaging time of 5.5 hours. This was shorter than the time required for histopathologic evaluation. Lesions depicted on the MR images were easily found in the histopathologic specimen, with the exception of lesions suspected on sections lost due to artifacts. Even small, inflammatory lesions found on the histologic sections were identified on MR imaging. Overall, lesion extent in the white matter, as shown on MR imaging and histopathologic analysis, was well correlated. However, inflammation present in gray matter was not detectable on the T2*-weighted MR images, as the signal intensity of gray matter and that of inflammatory lesions were virtually identical. Because gray matter lesions contributed little to the overall lesion load in this EAE model, the white matter lesion load, as measured with MR imaging, described the extent of disease in the examined samples well.

Histopathologic analysis is the criterion standard for the analysis of inflammation and demyelination in EAE. Histologic specimens are usually cut in 4–8-μm sections, resulting in a large number of sections per animal. Time constraints do not allow a comprehensive quantitative analysis of serial sections for most purposes. Sample distortion and disruption or processing artifacts additionally compromise the quantification and assessment of complex spatial relationships by means of histopathologic analysis. Therefore, semiquantitative analysis for inflammation is usually done by selecting a limited number of sections per spinal cord or brain sample and by counting the number of infiltrates per section and grading the infiltrates by the number of cell layers, for example. Other studies use image analysis software to delineate the area of inflammation on selected sections to determine the lesion volume in the whole sample. However, these methods provide only a rough estimate of the load of inflammation.

Our findings show that MR imaging represents a complementary tool with the potential to rapidly assess lesion pathology. In contrast to histopathologic analysis, MR imaging allows the acquisition of 3D MR image volumes in multiple phases of visualization and evaluation by using different imaging parameters without destroying the specimen; this allows for subsequent histopathologic analysis. Combining MR imaging with histopathologic analysis has several advantages: First, the MR imaging data allowed us to select particular areas of interest in the sample for a detailed histopathologic examination. Second, rapid 3D reconstruction and visualization was possible with the acquired MR imaging data. In contrast, serially analyzed histopathologic sections must be aligned in a time-consuming procedure, with many sections being skipped because of artifacts. Third, using these 3D MR datasets, we were able to quickly calculate the lesion load of the sample after semiautomatic segmentation.

Spatial resolution in MR microscopy is now approaching the dimensions used in histopathologic analysis. In our experiments, there was still potential for improvement of spatial resolution if we sacrificed a portion of the CNR. Because microscopic scans are usually run overnight, imaging time can be extended to increase the in-plane resolution during routine applications.

When MR imaging is performed on fixed tissue, imaging time is not the limiting factor. Therefore, an equivalent resolution with reasonable SNR can also be achieved with lower-field systems in a longer imaging time. Systems operating at 9.4 and 11.7 T are especially interesting for this application, since they have become more widely available and are now frequently used. With their relatively high field strength, measurements can still be done in a reasonable total imaging time. Since relaxation times are dependent on field strength, the contrast between healthy tissue and diseased tissue might differ at those frequencies.

A previous *ex vivo* study in murine spinal cords at 11.7 T achieved a spatial resolution comparable to ours (19). In that study, a different model with predominantly inflammatory lesions and little demyelination was used. While studies of rat spinal cord may obtain more structural information simply because of the substantially larger spinal cord in rats, the comparison of lesion morphology in various EAE models known to be pathogenetically heterogeneous may also prove to be helpful in understanding the striking heterogeneity of MR lesion morphology in MS.

The spatial resolution obtained here, in combination with semiautomatic lesion load quantification, offers researchers a rapid and convenient way of assessing experimental therapeutic effects on inflammatory lesion load in EAE. Only exemplary histologic evaluation focusing on differentiation of the various types of tissue damage is needed in addition. *In vivo* imaging will allow serial scanning of individual animals over the course of the disease and at defined time points in therapeutic trials. This advantage can potentially reduce the number of animals required to evaluate new experimental therapies. However, we postulate that the main advantage of the high spatial resolution will be seen after advanced techniques

(e.g., magnetization transfer and diffusion tensor imaging or use of targeted contrast agents) are established. These can potentially allow for more specific lesion characterization in various models of spinal cord damage. Imaging-driven lesion profiling in animal models might provide invaluable insights into how we can develop more specific sequences for *in vivo* characterization of pathologically defined lesions types in MS and other spinal cord diseases.

Conclusion

Ex vivo high-resolution MR microscopy of the spinal cord at 17.6 T allows excellent visualization of spinal cord inflammation. Virtually all inflammatory white matter lesions could be detected with a T2*-weighted gradient-echo sequence, as compared with histopathologic findings. Using a semiautomatic segmentation of the acquired MR imaging data, we could rapidly determine the white matter lesion load. Because of the lack of contrast difference between the lesions and healthy tissue, gray matter inflammatory lesions could not be visualized.

References

1. McDonald WI, Compston A, Edan G, et al. **Recommended diagnostic criteria for multiple sclerosis: guidelines from the International Panel on the Diagnosis of Multiple Sclerosis.** *Ann Neurol* 2001;50:121–127
2. Filippi M, Dousset V, McFarland HF, et al. **Role of magnetic resonance imaging in the diagnosis and monitoring of multiple sclerosis: consensus report of the White Matter Study group.** *J Magn Reson Imaging* 2002;15:499–504
3. Lycklama a Nijeholt G, Barkhof F. **Differences between subgroups of MS: MRI findings and correlation with histopathology.** *J Neurol Sci* 2003;206:173–174
4. Filippi M, Grossman RI. **MRI techniques to monitor MS evolution: the present and the future.** *Neurology* 2002;58:1147–1153
5. Lucchinetti C, Bruck W, Parisi J, et al. **Heterogeneity of multiple sclerosis lesions: implications for the pathogenesis of demyelination.** *Ann Neurol* 2000;47:707–717
6. Storch MK, Stefferl A, Brehm U, et al. **Autoimmunity to myelin oligodendrocyte glycoprotein in rats mimics the spectrum of multiple sclerosis pathology.** *Brain Pathol* 1998;8:681–694
7. Gold R, Hartung HP, Toyka KV. **Animal models for autoimmune demyelinating disorders of the nervous system.** *Mol Med Today* 2000;6:88–91
8. Lock C, Hermans G, Pedotti R, et al. **Gene-microarray analysis of multiple sclerosis lesions yields new targets validated in autoimmune encephalomyelitis.** *Nat Med* 2002;8:500–508
9. Hawkins CP, Mackenzie F, Tofts P, et al. **Patterns of blood-brain barrier breakdown in inflammatory demyelination.** *Brain* 1991;114: 801–810
10. Karlik SJ, Grant EA, Lee D, et al. **Gadolinium enhancement in acute and chronic progressive experimental allergic encephalomyelitis in the guinea pig.** *Magn Reson Med* 1993;30:326–331
11. Seeldrayers PA, Syha J, Morrissey SP, et al. **Magnetic resonance imaging investigation of blood-brain barrier damage in adoptive transfer experimental autoimmune encephalomyelitis.** *J Neuroimmunol* 1993;46:199–206
12. Morrissey SP, Stodal H, Zettl U, et al. **In vivo MRI and its histological correlates in acute adoptive transfer experimental allergic encephalomyelitis: quantification of inflammation and oedema.** *Brain* 1996;119:239–248
13. Verhoye MR, Gravenmade EJ, Raman ER, et al. **In vivo noninvasive determination of abnormal water diffusion in the rat brain studied in an animal model for multiple sclerosis by diffusion-weighted NMR imaging.** *Magn Reson Imaging* 1996;14:521–532
14. Dousset V, Delalande C, Ballarino L, et al. **In vivo macrophage activity imaging in the central nervous system detected by magnetic resonance.** *Magn Reson Med* 1999;41:329–333
15. Xu S, Jordan EK, Brocke S, et al. **Study of relapsing remitting experimental allergic encephalomyelitis SJL mouse model using MION-46L enhanced in vivo MRI: early histopathological correlation.** *J Neurosci Res* 1998;52:549–558
16. Rausch M, Hiestand P, Baumann D, et al. **MRI-based monitoring of inflammation and tissue damage in acute and chronic relapsing EAE.** *Magn Reson Med* 2003;50:309–314
17. Bulte JW, Douglas T, Witwer B, et al. **Magnetodendrimers allow endosomal magnetic labeling and in vivo tracking of stem cells.** *Nat Biotechnol* 2001;19:1141–1147
18. Lanens D, Van der Linden A, Gerrits PO, et al. **In vitro NMR micro imaging of the spinal cord of chronic relapsing EAE rats.** *Magn Reson Imaging* 1994;12:469–475
19. Ahrens ET, Laidlaw DH, Readhead C, et al. **MR microscopy of transgenic mice that spontaneously acquire experimental allergic encephalomyelitis.** *Magn Reson Med* 1998;40:119–132
20. Amor S, Groome N, Linington C, et al. **Identification of epitopes of myelin oligodendrocyte glycoprotein for the induction of experimental allergic encephalomyelitis in SJL and Biozzi AB/H mice.** *J Immunol* 1994;153:4349–4356
21. Haase A, Frahm J, Mathaei D, et al. **FLASH imaging: rapid NMR imaging using low flip-angle pulses.** *J Magn Reson Imaging* 1986;67: 258–267
22. Paxinos G, Watson C. *The Rat Brain in Stereotaxic Coordinates.* 4th ed. New York: Academic Press; 1998
23. Gareau PJ, Rutt BK, Karlik SJ, et al. **Magnetization transfer and multicomponent T2 relaxation measurements with histopathologic correlation in an experimental model of MS.** *J Magn Reson Imaging* 2000;11:586–595
24. Namer IJ, Mauss Y, Gounot D, et al. **NMR studies in demyelinating and nondemyelinating experimental allergic encephalomyelitis: an approach involving a dehydration procedure.** *Eur Neurol* 1999; 41:24–30